

Effective-Range Dependence of Resonantly Interacting Fermions

Michael McNeil Forbes,^{1,2} Stefano Gandolfi,³ and Alexandros Gezerlis^{2,4,5}

¹*Institute for Nuclear Theory, University of Washington, Seattle, Washington 98195-1550 USA*

²*Department of Physics, University of Washington, Seattle, Washington 98195-1560 USA*

³*Theoretical Division, Los Alamos National Laboratory, Los Alamos, New Mexico 87545, USA*

⁴*ExtreMe Matter Institute (EMMI), GSI Helmholtzzentrum für Schwerionenforschung GmbH, 64291 Darmstadt, Germany and*

⁵*Institut für Kernphysik, Technische Universität Darmstadt, 64289 Darmstadt, Germany*

(Dated: Friday 12th November, 2021)

We extract the leading effective range corrections to the equation of state of the unitary Fermi gas from *ab initio* Fixed-Node Quantum Monte Carlo (FNQMC) calculations in a periodic box using a Density Functional Theory (DFT), and show them to be universal by considering several two-body interactions. Furthermore, we find that the DFT is consistent with the best available unbiased QMC calculations, analytic results, and experimental measurements of the equation of state. We also discuss the asymptotic effective-range corrections for trapped systems and present the first QMC results with the correct asymptotic scaling.

PACS numbers: 67.85.-d, 71.15.Mb, 31.15.E-, 03.75.Ss, 24.10.Cn, 03.75.Hh, 21.60.-n

arXiv:1205.4815v2 [cond-mat.quant-gas] 15 Nov 2012

THE FERMION MANY-BODY PROBLEM plays a fundamental role in a vast array of physical systems, from dilute gases of cold atoms to nuclear physics in nuclei and neutron stars. The universal character of this problem – each system is governed by a similar microscopic theory – coupled with direct experimental access in cold atoms, has led to an explosion of recent interest (see Refs. [1] for reviews). Despite this broad applicability, we still do not fully understand even the simplest system: the “unitary gas” comprising equal numbers of two fermionic species with a resonant *s*-wave interaction of infinite scattering length $a_s \rightarrow \infty$. Lacking any scale beyond the total density $n_+ = n_a + n_b$, the unitary gas admits no perturbative expansion and requires experimental measurement or accurate numerical simulation for a quantitative description. Typical Quantum Monte Carlo (QMC) calculations, however, can access at most a few hundred particles, while experiments can measure only a handful of properties. Density Functional Theory (DFT) provides a complementary approach through which one may extrapolate these results to large systems beyond the reach of direct simulation. The question of how the unitary gas approaches the thermodynamic limit has also been studied in [2–5].

In this paper, we consider the effects of a finite effective range r_e on the unitary gas. Our motivation is two-fold. First, neutron matter – well approximated by a unitary gas [6] – differs primarily due to a finite range. Characterizing the finite range effects therefore have physical relevance. Second, we wish to directly use a DFT – a finite-range version of the Superfluid Local Density Approximation (SLDA) – to fit QMC simulations and extract thermodynamic properties without having to first extrapolate to zero range as was done in [3]. Directly fitting the finite range QMC data provides a much more stringent test of the SLDA. We use this finite-range DFT to extrapolate to the thermodynamic limit the linear range dependence of the equation of state, and

demonstrate its universality by simulating three different potentials. Two of the potentials include a repulsive core to address issues of contamination by deep bound states. We also show that the SLDA consistently fits all available unbiased zero-range *ab initio* results for the symmetric unitary gas. Finally, we present QMC results for trapped systems that demonstrate the correct asymptotic scaling as predicted by the low energy effective theory for the unitary gas.

Here we consider symmetric $T = 0$ systems comprising equal numbers of two neutral Fermi species with equal mass with a short-range interaction. These systems are directly realized by two of the lowest lying hyperfine states of ⁶Li in cold atomic systems, and approximately realized in dilute neutron-rich matter in the crusts of neutron stars. At sufficient dilution, the interaction can be characterized by the two-body *s*-wave phase shifts through the effective range expansion (see for example [7])

$$k \cot \delta_k = \frac{-1}{a_s} + \frac{r_e k^2}{2} + \mathcal{O}(k^4) \quad (1)$$

where a_s is the *s*-wave scattering length and r_e is the effective range. The zero-range unitary limit is realized when the scattering length is tuned $a_s \rightarrow \infty$ and the system is diluted such that $kr_e \rightarrow 0$: this is referred to as the symmetric Unitary Fermi Gas (UFG).

The lack of scales implies that the symmetric UFG is fully characterized by the universal Bertsch parameter [8] $\xi_S = \mathcal{E}/\mathcal{E}_{FG}$, where $\mathcal{E}_{FG} = (3/5)n_+ E_F$ is the energy density of a free Fermi gas with the same total density $n_+ = k_F^3/(3\pi^2)$, and $E_F = \hbar^2 k_F^2/2m$ is the Fermi energy.

In ⁶Li cold-atom experiments (see [9] for details), $a_s \approx \infty$ can be tuned using the wide magnetic Feshbach resonance at 834.1(15) G [10] with an effective range of $r_e \approx 4.7$ nm, while the gas can be cooled at densities of $1/k_F \approx 400$ nm so that $k_F r_e \approx 0.01$. In dilute neutron matter $a_{nn} \approx -18.9(4)$ fm [11] and $r_{nn} \approx 2.75(11)$ fm [12],

while densities are on the order of $1/k_F \sim 1$ fm: thus, $k_F r_e \approx 3$ is several orders of magnitude larger than in cold-atom systems.

Although there are formal ways of dealing with the divergences introduced by the zero-range limit (see [13] for an interesting approach), most *ab initio* calculational techniques require an explicit regulator in the form of a finite-range potential or a lattice cutoff. To extract the unitary parameters thus requires an extrapolation to zero effective range. Range effects in the UFG are also discussed in [14] (large r_e), [4] (Fixed-Node QMC (FNQMC)), and in [15, 16] (Bogoliubov-de Gennes (bdG) approximation).

I. SUMMARY

Here we present a summary of our results. We use a variational FNQMC algorithm to find upper bounds on the energy for systems of 4 to 66 particles in a periodic box for a variety of effective ranges $k_F r_e \lesssim 0.3$ and for different potentials with the same scattering length $a_s = \infty$ and range. We fit these directly with a modified DFT that models the range dependence in order to extrapolate to the thermodynamic an upper bound on the Bertsch parameter ξ , and the leading order universal effective range dependence ζ_e :

$$\begin{aligned} \xi(k_F r_e) &\lesssim \xi^* + \zeta_e^* k_F r_e + \mathcal{O}(k_F r_e)^2 \\ \xi^* &= 0.3897(4) \quad \zeta_e^* = 0.127(4). \end{aligned} \quad (2a)$$

By comparing several potentials, we confirm that these are indeed universal. The FNQMC results contain a systematic error due to the variational nature of the method. To better understand this, we also fit with the DFT a collection of unbiased exact, QMC, and experimental results for systems with 2 to 10^6 particles, obtaining a best fit of

$$\xi_S = 0.3742(5). \quad (2b)$$

We also demonstrate for the first time, QMC results for trapped systems that exhibit the correct asymptotic behavior in the thermodynamic limit.

II. QMC MODEL

We use a FNQMC algorithm to simulate the Hamiltonian

$$\mathcal{H} = \frac{\hbar^2}{2m} \left(- \sum_{k=1}^{N_+} \nabla_k^2 - \sum_{i,j'} V(r_{ij'}) \right), \quad (3)$$

where $V(r)$ is an inter-species interaction (off-resonance intra-species interactions are neglected). The FNQMC algorithm projects out the state of lowest energy from the space of all wave functions with fixed nodal structure as defined by an initial many-body wave function (ansatz).

By varying the Ansatz, we obtain an upper bound on the ground-state energy.

We use the trial function introduced in [17]:

$$\Psi_T = \mathcal{A}[\phi(\mathbf{r}_{11'})\phi(\mathbf{r}_{22'}) \cdots \phi(\mathbf{r}_{n n'})] \prod_{ij'} f(r_{ij'}),$$

where \mathcal{A} antisymmetrizes over particles of the same spin (either primed or unprimed) and $f(r)$ is a nodeless Jastrow function introduced to reduce the statistical error. The antisymmetrized product of s -wave pairing functions $\phi(\mathbf{r}_{ij'})$ defines the nodal structure:

$$\phi(\mathbf{r}) = \sum_{\mathbf{n}} \alpha_{\|\mathbf{n}\|} e^{i\mathbf{k}_{\mathbf{n}} \cdot \mathbf{r}} + \tilde{\beta}(\mathbf{r}).$$

The sum is truncated (we include ten coefficients) and the omitted short-range tail is modelled by the phenomenological function $\tilde{\beta}(\mathbf{r})$ chosen to ensure smooth behavior near zero separation. We use the same form for $\tilde{\beta}(\mathbf{r})$ as in [18] and vary the 10 coefficients $\alpha_{\|\mathbf{n}\|}$ for each N_+ and for each different two-body potential to minimize the energy as described in Ref. [19]. The same ansatz suffices for different effective ranges, but an independent optimization is required for each N_+ .

We compare the following potentials:

$$V_{PT}(r) = 4\mu^2 \operatorname{sech}^2(\mu r), \quad (4a)$$

$$V_{2G}(r) = 3.144\mu^2 \left(e^{-\mu^2 r^2/4} - 4e^{-\mu^2 r^2} \right), \quad (4b)$$

$$V_{2E}(r) = 4.764\mu^2 \left(e^{-\mu r} - 2e^{-2\mu r} \right). \quad (4c)$$

These potentials are all tuned to have infinite two-body s -wave scattering length. The first potential (4a) is of the modified-Pöschl-Teller type; the second (4b) and third (4c) potentials have a repulsive core. When tuned to unitarity, the effective range r_e is proportional to μ^{-1} as shown in figure 1.

One criticism of purely attractive potentials – including the widely used modified-Pöschl-Teller potential (4a) – is that they may contain deeply bound states where many particles lie within the range of the potential. Formally, the ground state is thus not the universal dilute

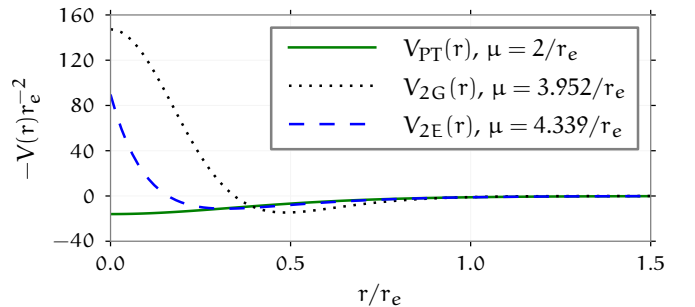


Figure 1. (color online) Finite range potentials (4) used in the Hamiltonian (3) for our QMC bounds.

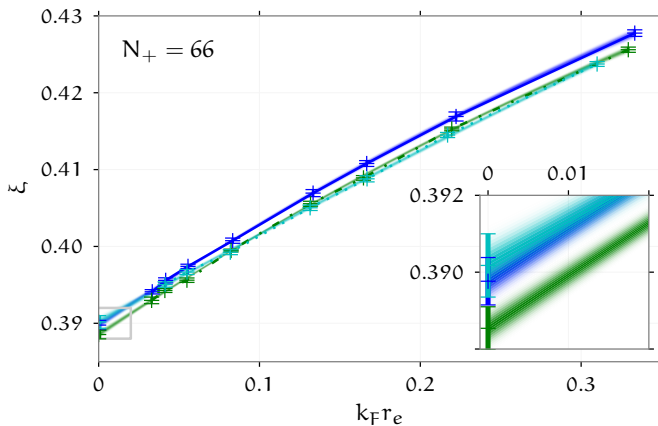


Figure 2. (color online) Effective range dependence of the ground-state energy-density $\xi(k_{\text{F}}r_e) = \varepsilon/\varepsilon_{\text{FG}}$ of $N_+ = 66$ fermions in a periodic cubic box in the unitary limit. The points with error-bars are the raw QMC results and the bands are the 1σ error bands of polynomial fits. The upper (blue) curve that extrapolates to $\xi = 0.3898(5)$ is the new quadratic fit to the modified-Pöschl-Teller potential (4a). The middle (green) curve that extrapolates to $\xi = 0.3885(5)$ is the quadratic fit for the new double-Gaussian potential (4b). Finally, the lower (cyan) curve that extrapolates to $\xi = 0.3902(7)$ is the quadratic fit to the double-exponential potential (4c).

UFG, but some tightly bound state that is highly sensitive to the range. In principle, this state may contaminate the variational QMC calculation, but in practice, there is insufficient overlap between the variational wave function and this deep bound state. (Simulations longer by several orders of magnitude would be required to see the influence of such low-energy states.)

The repulsive cores of (4b) and (4c) help allay these concerns by reducing the possibility of contamination from deeply bound states. We find agreement between the purely attractive Pöschl-Teller potential and these repulsive potentials, demonstrating that all three potentials may be used to calculate properties of the UFG, and verifying the model-independence of the universal parameters. We show the upper bounds for the energy of $N_+ = 66$ particles at various effective ranges in figure 2. For ranges less than $k_{\text{F}}r_e \lesssim 0.3$ a three-parameter quadratic model is sufficient to extrapolate to zero range without a systematic bias. This fit is shown in table I for the three potentials, and the magnitude of the quadratic parameter can be used to estimate the linear regime.

In [3], each N_+ was independently extrapolated to zero effective range, then the unitary SLDA DFT was fit to the extrapolated results. It was claimed that a cubic fit was required to extrapolate the results for $k_{\text{F}}r_e < 0.35$ to zero range, however, the smallest ranges $k_{\text{F}}r_e < 0.1$ had a small systematic bias in the energy due to the Trotter decomposition of the many-body propagator $e^{-\hat{H}\delta\tau} \approx e^{-\hat{V}\delta\tau/2}e^{-\hat{K}\delta\tau}e^{-\hat{V}\delta\tau/2} + \mathcal{O}(\hat{V}\delta\tau)^3$ where $\delta\tau/\hbar$ is the imaginary time-step. Since the potentials (4) scale

roughly as $\hat{V} \propto \mu^2 \propto r_e^{-2}$, for small ranges, one needs a very small imaginary time-step, which is computationally expensive. The extrapolated values of ξ were only underestimated for the larger systems (by $\sim 3\%$), but extracting the slope of $\xi(k_{\text{F}}r_e)$ requires higher accuracy. Here we have carefully simulated with smaller time-steps (for the ranges considered here, $\delta\tau\varepsilon_{\text{F}} \approx 5 \times 10^{-6}$ is sufficient to avoid any bias) to find that, for $k_{\text{F}}r_e \lesssim 0.3$, a quadratic (but not linear) fit is sufficient. We also no longer use an independent zero-range extrapolation for each N_+ . Instead, we use a generalized finite-range-SLDA to fit all of the finite-range-QMC results with a common set of parameters. This requires simultaneous consistency over all ranges *and* all particle numbers, providing a more rigorous test than independently extrapolating each N_+ .

III. SLDA DFT WITH FINITE RANGE

As was shown in [3], the finite-size (“shell”) effects in $\xi_{\text{S}}(N_+)$ can be well modelled by a simple local DFT for the unitary Fermi gas, but are not even qualitatively reproduced by adding only gradient or kinetic corrections [21–23]. In this paper we retain the same three-parameter form originally introduced in Ref. [24] (called the SLDA), but present a simple generalization that accounts for finite-range effects. With this generalized form, we can directly fit the QMC results without the need to first extrapolate to zero range. We first briefly review the form of the SLDA DFT, then discuss the finite-range generalization.

The SLDA DFT is formulated in terms of three local densities (see [25] for a review): the total density n_+ , the

	$\xi_{66} (= a_0)$	$\zeta_e(66) (= a_1)$	a_2	χ_{F}^2
V_{PT}	0.3898(4)	0.14(1)	-0.07	0.20
$V_{2\text{G}}$	0.3885(4)	0.14(1)	-0.08	0.40
$V_{2\text{E}}$	0.3902(5)	0.12(1)	-0.03	0.30

Table I. Comparison of the zero-range extrapolations of $\varepsilon(k_{\text{F}}r_e)/\varepsilon_{\text{FG}} = \xi_{66} + \zeta_e(66)k_{\text{F}}r_e + a_2(k_{\text{F}}r_e)^2 + \mathcal{O}(r_e^3)$ for quadratic fits of the $N_+ = 66$ QMC results. These values are higher than, but consistent with the value $\zeta_e(66) = 0.11(3)$ reported in [20]. The extrapolations of these parameters to the thermodynamic limit $N_+ = \infty$ are listed as $\xi = a_0$ and $\zeta_e = a_1$ in the ξ block of table II. We include the quadratic coefficient simply to show that the QMC can be fit using a linear form for $k_{\text{F}}r_e < \varepsilon_{\text{abs}}|a_1/a_2|$ to an absolute accuracy of about ε_{abs} : we do not have any a priori reason to believe that this parameter is universal. The systematic error due to neglecting the cubic terms is on the same order as the quoted 1σ statistical errors.

total kinetic density τ_+ , and an anomalous v :

$$\begin{aligned} n_+ &= 2 \sum_{\mathbf{n}} |v_{\mathbf{n}}|^2 \sim \langle \hat{a}^\dagger \hat{a} \rangle + \langle \hat{b}^\dagger \hat{b} \rangle, \\ \tau_+ &= 2 \sum_{\mathbf{n}} |\nabla v_{\mathbf{n}}|^2 \sim \langle \vec{\nabla} \hat{a}^\dagger \cdot \vec{\nabla} \hat{a} \rangle + \langle \vec{\nabla} \hat{b}^\dagger \cdot \vec{\nabla} \hat{b} \rangle, \\ v &= \sum_{\mathbf{n}} u_{\mathbf{n}} v_{\mathbf{n}}^* \sim \langle \hat{a} \hat{b} \rangle. \end{aligned}$$

These are expressed in terms of the Bogoliubov quasiparticle wave functions $u_{\mathbf{n}}(\mathbf{r})$ and $v_{\mathbf{n}}(\mathbf{r})$ – sometimes called “coherence factors”.

The three-parameter SLDA may then be expressed as

$$\mathcal{E}_{\text{SLDA}} = \frac{\hbar^2}{m} \left(\frac{\alpha}{2} \tau_+ + \beta \frac{3}{10} (3\pi^2)^{2/3} n_+^{5/3} \right) + g v^\dagger v,$$

where $\alpha = m/m_{\text{eff}}$ parametrizes the inverse effective mass; β parametrizes the self-energy; and g parametrizes the pairing interaction. In the presence of pairing, the local kinetic and anomalous densities are divergent

$$\begin{aligned} \lim_{\delta \rightarrow 0} v(\vec{x}, \vec{x} + \vec{\delta}) &\rightarrow \frac{A_v}{\delta} + v_r(\vec{x}) + \mathcal{O}(\delta), \\ \lim_{\delta \rightarrow 0} \tau_+(\vec{x}, \vec{x} + \vec{\delta}) &\rightarrow \frac{A_\tau}{\delta} + \tau_r(\vec{x}) + \mathcal{O}(\delta), \end{aligned}$$

where A_v , A_τ , v_r and τ_r are finite. One must regulate the theory if one wishes to maintain a local formulation, which greatly simplifies the computational aspects of the DFT. The most general form of a local functional involving these three densities is a function of these four finite quantities, but restricting the form to bounded functionals is somewhat non-trivial [26], and we shall not consider these generalizations here.

We note that the $1/\delta$ divergence corresponds to a long $1/k^2$ momentum tail in the Fourier transform of the anomalous and kinetic densities. This follows from the short-range nature of the potential as has been emphasized by Tan [13]. The most straightforward route is to simply introduce a momentum cutoff $k < k_c$ and then define the theory in the limit of large cutoff. The local densities then behave as

$$\tau_+ = A_\tau \Lambda + \tau_r + \mathcal{O}(\Lambda^{-1}), \quad v = A_v \Lambda + v_r + \mathcal{O}(\Lambda^{-1}),$$

where $\Lambda = \int k^{-2} d^3k / (2\pi)^3 = k_c / 2\pi^2$. Within the single-particle framework of the DFT, these are related to the gap Δ : $A_\tau = 2m|\Delta|^2/\alpha^2$, and $A_v = \Delta/\alpha$. Similar short-range behavior is expected in the physical density distributions where the coefficients A_τ and A_v are related to the Tan’s “contact” C – for example, $A_v = \sqrt{2C}/2m$ – and it is tempting to interpret $\sqrt{2C} \approx 2m\Delta/\alpha$ as a prediction of the DFT, especially at unitarity where they seem to be related numerically. This cannot hold in general: in particular, the contact C is related to the short-range nature of the interaction and persists in the normal phase (either meta-stable or above the critical temperature $T > T_c$)

where the order parameter Δ vanishes [27]. The inverse coupling constant may be expressed

$$g^{-1} = n_+^{1/3}/\gamma - \Lambda/\alpha,$$

where γ is the third dimensionless parameter characterizing the SLDA.

The equations of motion follow by minimizing the total energy $E = \int d^3x \mathcal{E}_{\text{SLDA}}$ with respect to the occupation factors u and v subject to the constraints of fixed total particle number N_+ and normalization. This leads to the following single-particle Hamiltonian for the Bogoliubov quasiparticle wavefunctions:

$$\begin{pmatrix} K & \Delta^\dagger \\ \Delta & -K \end{pmatrix} \begin{pmatrix} u_{\mathbf{n}} \\ v_{\mathbf{n}} \end{pmatrix} = E_{\mathbf{n}} \begin{pmatrix} u_{\mathbf{n}} \\ v_{\mathbf{n}} \end{pmatrix}, \quad K = \hbar^2 \frac{-\vec{\nabla} \alpha \vec{\nabla}}{2m} - \mu + U$$

where $U = \partial \mathcal{E} / \partial n_+$, and $\Delta = -gv$. These must be solved self-consistently to find the stationary configurations. With infinite cutoff, the self-consistency equations become

$$U = \beta E_F - \frac{|\Delta|^2}{3n_+^{3/2}\gamma}, \quad \Delta = -\gamma \frac{v_r}{n_+^{1/3}}.$$

The mean-field BdG equations may be recovered by setting $\alpha = 1$, $\beta = 0$, and replacing $n_+^{1/3}/\gamma = 4\pi/a$. The resulting functional contains no explicit density dependence, and so contains no self-energy $U = 0$. The SLDA differs from the BdG equations by the inclusion of an effective mass and a self-energy.

The SLDA functional is defined by the three dimensionless constants α , β , and γ . In practice, we use the homogeneous solution to the gap equation in the thermodynamic limit to replace β and γ with the more physically relevant parameters

$$\alpha \equiv \frac{m}{m_{\text{eff}}}, \quad \xi \equiv \frac{\mathcal{E}}{\mathcal{E}_{\text{FG}}}, \quad \eta \equiv \frac{\Delta}{\overline{E}_F}$$

as discussed in detail in appendix A [see Eq. A4].

To extend the functional to finite range, we simply let the three parameters α , ξ , and η depend on the dimensionless combination $k_{\text{F}r_e}$. This introduces an additional explicit density dependence in the functional through $k_{\text{F}} \propto n_+^{1/3}$ and the self-energy must be modified accordingly. The use of the nonlinear relationships (A4) between the polynomial form for $\alpha(k_{\text{F}r_e})$, $\eta(k_{\text{F}r_e})$, and $\xi(k_{\text{F}r_e})$ and the parameters of the function makes this complicated to write down, but numerically it is straightforward to propagate these derivatives using, for example, automatic differentiation tools such as THEANO [28].

For the small ranges considered in this paper, we find that a quadratic parametrization suffices:

$$\alpha, \xi, \eta = a_0 + a_1 k_{\text{F}r_e} + a_2 (k_{\text{F}r_e})^2.$$

(Including higher order terms leads to no significant improvement in the quality of the fits.) This finite-range-SLDA thus has 9 independent parameters – the three

coefficients a_n for each of the parameters α , ξ , and η . In comparison, the procedure of independently extrapolating each N_+ to zero range introduces 3 new parameters for each N_+ in addition to the three SLDA parameters, effecting a significant increase in the total number of fitting parameters. Note also that the new fits directly use the QMC results – including their sub-percent statistical errors – rather than the extrapolated error bar from zero-range extrapolation: thus the new fitting procedure places the SLDA under a significantly more stringent test.

We only expect this extension to model the effective-range dependence in universal regions. In particular, a true finite-range interaction would naturally regulate the system, eschewing the need for an additional cutoff in the DFT. For example, in the mean-field approximation, the use of a finite-range separable potential $g v_k v_q$ with decaying form-factors gives rise to a momentum-dependent gap $\Delta_k \propto v_k$ regulating the anomalous density at large momenta. Introducing such a natural regulation into the DFT, however, will likely require the introduction of some form of non-locality, which significantly complicates the computational aspects of the theory.

In principle, one could also introduce a dependence on the scattering length a and temperature T in a similar manner, making the coefficients functions of $k_F a$ and $k_B T/E_F$ respectively. Unlike the case with the effective range, however, the dependence on these parameters must be modelled for all values since the unitary limit corresponds to $k_F a = \pm\infty$ and $T/E_F = 0$, while for finite a and T , the zero-density limit (at the edge of a trapped cloud for example) is described by $k_F a = 0$ and $T/E_F = \infty$; hence, any physical system close to unitarity explores virtually all values of these functions, requiring a careful and complete characterization.

IV. RESULTS

A. Box

The results of this 9-parameter fit to the QMC data-points with effective ranges $0.03 < k_F r_e \leq 0.33$ are shown in table II. The fit to 60 points with $4 \leq N_+ \leq 130$ for the V_{2G} potential has a reduced chi squared $\chi_r^2 = 5$. The fit to 70 points for $4 \leq N_+ \leq 130$ to the V_{PT} potential has $\chi_r^2 = 7$. We suspect that this is due to approximating the effective range dependence with a purely local functional as discussed earlier.

As before [3], the best fit gap parameter η and inverse effective mass α are inconsistent with the values $\eta = 0.50(5)$ and $\alpha = 1.09(2)$ obtained from the $N_+ = 66$ QMC quasiparticle dispersion relation [29, 30], and the values $\eta = 0.45(5)$ [31] and $\eta = 0.44(3)$ [32] extracted from experimental data. As we shall see below (see Eq. 7), this may be due to the fixed-node approximation.

Linear	a_0	a_1	χ_r^2	
ξ_{PT}	0.3911(4)	0.111(3)	8	
ξ_{2G}	0.3900(3)	0.111(2)	6	
η_{PT}	0.90(1)	-0.85(7)		
η_{2G}	0.875(8)	-0.82(4)		
α_{PT}	1.303(10)	-0.71(8)		
α_{2G}	1.289(7)	-0.69(3)		
Quadratic	a_0	a_1	a_2	χ_r^2
ξ_{PT}	0.3903(7)	0.121(10)	0.00(3)	7
ξ_{2G}	0.3890(4)	0.128(4)	-0.06(1)	5
η_{PT}	0.99(3)	-2.1(4)	3(1)	
η_{2G}	0.879(7)	-0.84(3)	0.00(3)	
α_{PT}	1.34(2)	-1.6(4)	5(2)	
α_{2G}	1.292(7)	-0.73(6)	0.1(2)	

Table II. Best fit SLDA parameters for linear (quadratic) 6-parameter (9-parameter) models: coefficients a_0 , a_1 , (and a_2) for each parameter ξ , η , and α . Note that the parameters α and η should be positive, requiring positive higher-order terms that are not properly constrained by our QMC which only simulates $k_F r_e \lesssim 0.3$: larger ranges require higher-order polynomials (or a different model).

Werner and Castin [33] showed that the many-body energy density depends linearly on the effective range in the zero-range limit

$$\frac{\mathcal{E}}{\mathcal{E}_{FG}} = \xi_S + \zeta_e k_F r_e + \mathcal{O}((k_F r_e)^2) \quad (6)$$

where the coefficient ζ_e is a universal constant within Galilean invariant continuous space models. The value for this coefficient was first estimated $\zeta_e = 0.046(7)$ [34] by fitting (6) to the exact two-particle solution in a trap.

The value for this coefficient for $N = 66$ particles $\zeta_e(66) = 0.11(3)$ was calculated using Auxiliary Field QMC (AFQMC) in [20] (see table I for comparison) and is likely independent of other universal parameters such as ξ or the contact C [27]. The finite-range-SLDA allows us to extrapolate this result to the thermodynamic limit (see table II) where we find $\zeta_S = 0.127(4)$ by averaging the linear ξ coefficient a_1 for both V_{PT} ($\zeta_e = 0.121(10)$) and V_{2G} ($\zeta_e = 0.128(4)$) results. Note that these are consistent, demonstrating the universality of this coefficient.

Unfortunately, since the FNQMC can only provide an upper bound on the energy, ξ is systematically overestimated due to the nodal constraint. An improved nodal structure would lower all energies, however, and there is no a priori reason to suspect as large a bias for ζ_e .

To address the potential systematic error introduced by the fixed-node approximation, we apply the same analysis to the recent unbiased calculations and measurements shown in table III. These include zero-range extrapolations of two exact diagonalizations for $N_+ = 4$ [35], zero-range extrapolations of AFQMC results for

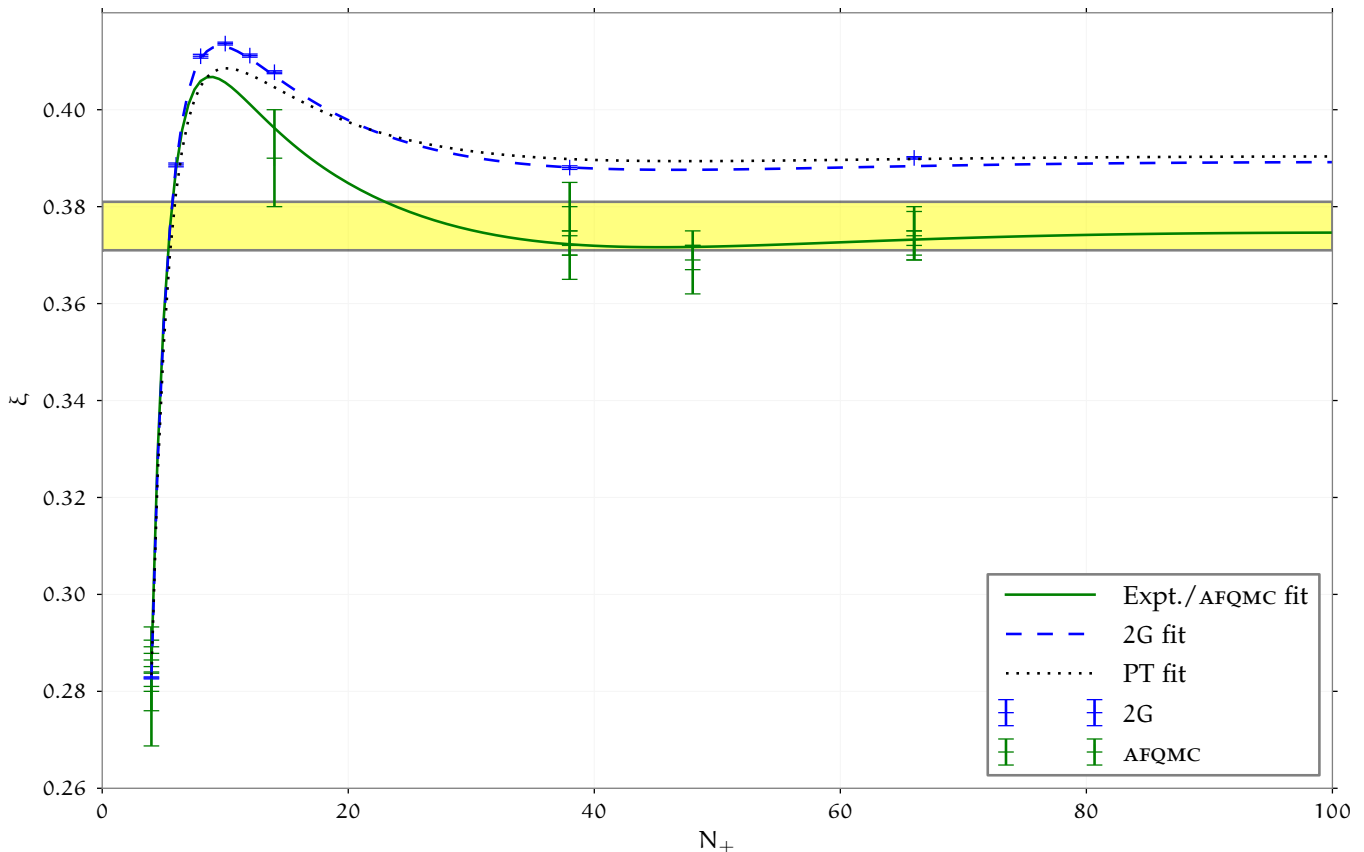


Figure 3. (color online) Comparison of SLDA fits at zero range with zero-range extrapolated QMC upper bounds (blue) with all unbiased zero-range extrapolations (green) from [20, 35] listed in table III. The light (yellow) band is the experimental value of ξ_S [9]. In addition, we fit the exact $\xi_2 = -0.4153\dots$ value discussed in appendix B (not shown in the plot). Note that this comparison allows one to assess the FNQMC bound, which is tight for $N_+ \leq 6$.

$N_+ = 4$ [35] and for $N_+ \in \{4, 14, 38, 48, 66\}$ [20], and experimental measurements of ${}^6\text{Li}$ for $N_+ \approx 10^6$ [9]. (Although not strictly at zero-range, the error induced by the non-zero range in the ${}^6\text{Li}$ experiments should be less than 0.003 (see also section IV B).)

We use these points to fit our three-parameter zero-range SLDA, finding:

$$\xi_S = 0.3742(5), \quad \alpha = 1.104(8), \quad \eta = 0.651(9). \quad (7)$$

These error estimates must be taken with a grain of salt since not all of the error bars quoted in table III are 1σ normal standard deviations. This is reflected in the rather small $\chi_r^2 = 0.2$ of the fit. The results of this full fit are shown in figure 3.

This partially addresses the suspiciously large value of η found by fitting FNQMC results (see table II). It appears that a large part of the previous discrepancy is due to the fixed-node approximation which works well for small systems, but systematically overestimates the energy of large systems. (The variational wavefunction has the same number of parameters for all system sizes, we therefore expect it to better match the simpler nodal structure of small systems than the more complicated

nodal structure of larger systems.) The gap η still appears to be too large, which may be a problem when one tries to fit odd systems.

N_+	ξ_{N_+}	Method
2	$-0.415332919\dots$	exact (see section B)
4	0.288(3), 0.286(3)	exact diagonalization [35]
4	0.28(1)	AFQMC [35]
4	0.280(4)	AFQMC [20]
14	0.39(1)	AFQMC [20]
38	0.370(5), 0.372(2), 0.380(5)	AFQMC [20]
48	0.372(3), 0.367(5)	AFQMC [20]
66	0.374(5), 0.372(3), 0.375(5)	AFQMC [20]
10^6	0.376(5)	experiment [9]

Table III. Unbiased zero-range box energies. Most are extrapolated AFQMC results except as noted. The ξ_4 values are consistent with our upper bounds 0.2839(3) (V_{PT}), and 0.2829(3) (V_{2G}). This agreement indicates that the systematic error due to the fixed-node constraint is sub-percent for $N_+ = 4$.

The results shown in Fig. 2 may help understand the finite-size effects seen in neutron matter and neutron drops. In neutron matter at $k_{Fa} = -10$ the difference

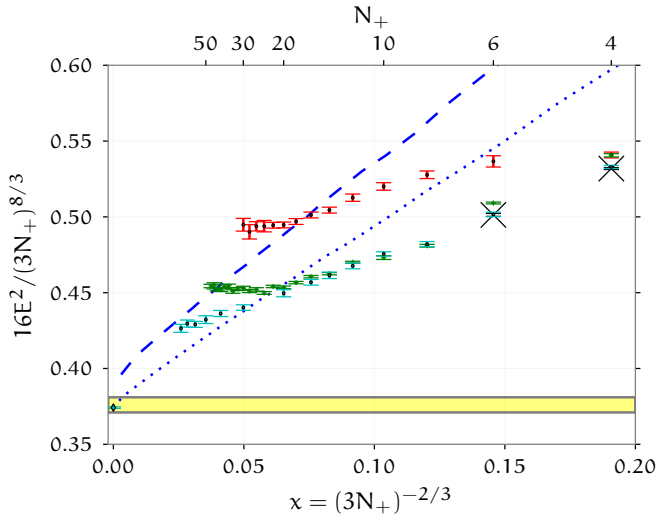


Figure 4. (color online) Ground-state energy of the harmonically trapped unitary Fermi gas (in units where $\hbar\omega = 1$) scaled to demonstrate the asymptotic form (9) predicted by the low-energy effective theory of Ref. [38]. The SLDA with quadratic fit in table II (dashed blue line) and unbiased fit (7) (dotted blue line) is compared with zero-range results for $N_+ \in \{4, 6\}$ from Ref. [39] (black xs), and finite-range QMC results from Ref. [40] (upper red dots) and Ref. [41] (middle green pluses). The latter have significantly lower energy, despite having a slightly larger effective range, suggesting that the wave functions in Ref. [40] were not fully optimized. A more thorough optimization and extrapolation to zero effective-range yields the lowest points (cyan dots) which exhibit the correct scaling at large N_+ , approaching the thermodynamic value of ξ . We also include at $x = 0$ the fit ξ from Eq. (7) (cyan diamond) and the light (yellow) experimental band [9].

between the energies of $N_+ = 20$ and $N_+ = 44$ particles is roughly 12% [36]. The range of $k_{\text{F}r_e}$ values shown in Fig. 2 is too limited to allow an accurate extrapolation to nuclear ranges. Even so, simple extrapolations of the energies of $N_+ = 14$ and $N_+ = 38$ particles to $k_{\text{F}r_e} = 1.45$ using linear and quadratic forms lead to shell effects on the order of 10-20%, which is consistent with the (finite scattering-length) results seen in neutron drops [37].

B. Harmonic Traps

As an application, we show here how the universal effective range dependence (6) affects the energy of particles in an isotropic harmonic trapping potential $V(r) = m\omega^2 r^2/2$ using the Thomas-Fermi (TF) approximation. The local chemical potential is $\mu(r) = \mu_0 - V(r)$, and the equation of state

$$\frac{\mu(r)}{E_{\text{F}}} = \xi_S + \frac{9}{5}\zeta_e k_{\text{F}r_e} + \dots$$

thereby establishes the local density and energy-density within the TF approximation out to the maximum TF

radius of $R = \sqrt{2\mu_0/m}/\omega$. Including these first two terms we thus obtain

$$N_+ = \frac{\omega^3 R^6}{24\xi^{3/2}} - \zeta_e r_e \frac{32\omega^4 R^7}{175\pi\xi^3} + \dots,$$

$$\frac{E}{\hbar\omega} = \frac{\omega^4 R^8}{64\xi^{3/2}} - \zeta_e r_e \frac{16\omega^5 R^9}{225\pi\xi^3} + \dots$$

In the zero-range limit, the energy of a trapped unitary gas may be calculated using the low-energy effective theory [38] and has the form

$$E = \hbar\omega \frac{1}{4}(3N_+)^{4/3} \left(\sqrt{\xi} + \right. \\ \left. - 6\sqrt{2}\pi^2 \xi(2c_1 - 9c_2)(3N_+)^{-2/3} + \mathcal{O}(N_+^{-7/9}) \right)$$

where the leading order term is the well-known TF expression (see for example [42]). The next-to-leading order term is directly related to the q^2 coefficient of the static-response and the coefficients have been estimated using the ϵ -expansion [22]. The asymptotic corrections are due to boundary effects beyond the validity of the effective theory.

This naturally suggests the introduction of the parameter $\chi = (3N_+)^{-2/3}$ so that the asymptotic behavior of E is linear in χ . The square of the energy E^2 also exhibits linear asymptotic behavior,

$$\frac{16E^2}{\hbar^2\omega^2(3N_+)^{8/3}} = \xi + c\chi + \mathcal{O}(\chi^{7/6}), \quad (9)$$

where $c = -12\sqrt{2}\pi^2\xi^{3/2}(2c_1 - 9c_2)$. We prefer this form as ξ appears as the intercept and note that the relationship is remarkably linear, as can be seen in figure 4.

It is interesting that, in the non-interacting system, shell-effects appear at the same linear order χ , leading to a fundamental uncertainty in the coefficient $0.67 < c < 1.7$. Pairing suppresses these shell effects, and they are virtually non-existent in the unitary gas leading to a well-defined value of c . Note that the TF approximation contains only the leading order term: i.e. $c = 0$.

In the TF approximation, the leading-order effective-range correction $\zeta_e k_{\text{F}r_e}$ leads to a super-leading order (in N_+) correction to (9):

$$\frac{16E^2}{\hbar^2\omega^2(3N_+)^{8/3}} = \xi + 1.17 \frac{\zeta_e r_e}{\xi^{1/4}} \sqrt{\omega} \chi^{-1/4} + \mathcal{O}(r_e^2). \quad (10)$$

(The coefficient is $1.17 = 2^{25/2}/1575\pi$.) The singular $\chi^{-1/4}$ demonstrates that, as N_+ gets large, the central density becomes large and $k_{\text{F}r_e}$ corrections play an increasingly significant role. The analysis is therefore only valid in a limited regime where the system is sufficiently large that the TF approximation is valid, but where the central density is small enough that $k_{\text{F}r_e}$ remains small. It illustrates how a finite effective range will alter the linear asymptotic behavior expected in figure 4.

In figure 4 we show new fixed-node QMC results that have been extrapolated to zero-range using a quadratic polynomial in k_{FRE} . These results represent the first *ab initio* calculations to demonstrate the correct linear asymptotic scaling as predicted by the effective theory. In particular, all previous results start to “turn up” as they approach the thermodynamic limit. While this is qualitatively consistent with the expected divergent $\chi^{-1/4}$ behavior expected of a finite-range, the effect does not agree quantitatively: eq. 10 predicts the divergence to set in at a larger N_+ than seen in figure 4. We suspect that the incorrect scaling of previous trapped results indicates the presence of spurious length scales (but in principle, could also signify spurious breaking of another symmetry).

Allowing a more flexible variational wavefunction (green pluses [41]) improves the bound compared with the red dots of [40]. This seems sufficient for small systems as witnessed by the agreement with the $N_+ \in \{4, 6\}$ results of [39], but does not provide the correct asymptotic behavior in larger traps where the density and pairing correlations differ substantially between the center and edges of the trap. To obtain the correct asymptotic behavior here, we include an explicit dependence on the center-of-mass coordinate of each pair in the variational pairing wavefunction (cyan dots).

The linear scaling of our new results indicates that this nodal approximation does not introduce any spurious length scales, however, even with this extra freedom, the variational bound provided for trapped systems is not as tight as it is for homogeneous matter, and the cyan dots extrapolate to a somewhat higher bound for the value of $\xi \approx 0.4$. As with the homogeneous systems, we find the same trend that the variational bound is tight for small systems, but is less accurate for larger systems where pairing correlations become more significant.

Finally, we have included the SLDA predictions in the figure 4 (blue curves) but do not use the SLDA to fit the results since we have not included any gradient corrections. By construction, the SLDA extrapolates to the thermodynamic value of ξ used in the parametrization, but the slope is sensitive to the leading order gradient corrections that we have neglected in this paper since they do not contribute to homogeneous matter. This plot contains within it hints as to the nature of the gradient corrections to the SLDA, but quantitative statements require further analysis beyond the scope of this paper.

V. SUMMARY AND CONCLUSIONS

In this work we have extensively analyzed the ground-state energy of strongly interacting atoms for finite effective ranges. We present new Fixed-Node QMC results for inter-atomic potentials that also contain repulsive cores: these new potentials yield results that are statistically consistent with the purely attractive (modified Pöschl-Teller) potential used in earlier works, demonstrating the universality of the leading finite-effective-range dependence, and addressing concerns about contamination of the FNQMC energies by deeply bound many-body states.

To model these results in a common framework, we have minimally extended the Superfluid Local Density Approximation Density Functional Theory to directly fit the finite-range FNQMC results. Although this simple generalization of the SLDA is not completely consistent with the FNQMC results, it still proves to be a useful tool for extrapolating finite-size results to the thermodynamic limit. To assess the accuracy of the variational upper bound provided by the FNQMC results, we have also fit the SLDA to unbiased (non-variational) exact, QMC, and experimental results from the literature to produce a working SLDA for modeling physical systems. This fit demonstrates that the three-parameter zero-range SLDA is consistent with the unbiased results.

Finally, we have presented new QMC results for zero-range trapped systems. These results demonstrate, for the first time, the correct asymptotic behavior in the thermodynamic limit as predicted by the low-energy effective theory.

ACKNOWLEDGMENTS

We thank A. Bulgac, J. Carlson, Y. Castin, Y. Nishida, and F. Werner for useful discussions. This work is supported, in part, by US Department of Energy (DOE) grants DE-FG02-00ER41132, DE-FG02-97ER41014, & DE-AC52-06NA25396, DOE contracts DE-FC02-07ER41457 (UNEDF SCIDAC) & DE-AC52-06NA25396, by the LDRD program at Los Alamos National Laboratory (LANL), by the Helmholtz Alliance Program of the Helmholtz Association HA216/EMMI. Computations for this work were carried out through Open Supercomputing at LANL, and at the National Energy Research Science Computing (NERSC).

Appendix A: Homogeneous solutions of the Superfluid Local Density Approximation

In this appendix, we describe some properties of homogeneous solutions to the SLDA functional, both in the periodic box, and in the thermodynamic limit of infinite matter. (When these equations are applied locally at each point in a slowly varying external potential, one obtains the TF approximation.) As discussed in the text, we use the thermodynamic solutions to express the parameters β and γ in terms of the more physically relevant quantities ξ and η .

We start by rotating away the phase, taking $\Delta = |\Delta|$ to be real. We also note that the self-energy U plays no role in the solution of the homogeneous equations: all effects are absorbed into the effective chemical potential μ_{eff} . One only needs to compute the self energy U to relate the effective chemical to the thermodynamic chemical potential. Thus, the homogeneous Hamiltonian is completely parametrized by α , μ_{eff} , and Δ . In momentum space, the Hamiltonian is easily diagonalized,

$$\mathbf{H} = \begin{pmatrix} \epsilon_k & \Delta \\ \Delta & -\epsilon_k \end{pmatrix} = \begin{pmatrix} u_k & v_k \\ v_k & -u_k \end{pmatrix} \begin{pmatrix} E_k & \\ & -E_k \end{pmatrix} \begin{pmatrix} u_k & v_k \\ v_k & -u_k \end{pmatrix},$$

$$\epsilon_k = \frac{\alpha \hbar^2 k^2}{2m} - \mu_{\text{eff}}, \quad E_k = \sqrt{\epsilon_k^2 + \Delta^2},$$

$$u_k = \sqrt{\frac{1 + \frac{\epsilon_k}{E_k}}{2}}, \quad v_k = \sqrt{\frac{1 - \frac{\epsilon_k}{E_k}}{2}}.$$

In this diagonal form, the density matrix $\rho = f_\beta(\mathbf{H})$ can be computed in a straightforward manner from the Fermi distribution function $f_\beta(\mathbf{H}) = 1/[1 + \exp(-\beta\mathbf{H})]$. For reference, the zero-temperature results are:

$$n_+(\alpha, \mu_{\text{eff}}, \Delta) = \int \frac{d^3\vec{k}}{(2\pi)^3} \left(1 - \frac{\epsilon_k}{E_k}\right),$$

$$\frac{\tau(\alpha, \mu_{\text{eff}}, \Delta)}{2m} = \int \frac{d^3\vec{k}}{(2\pi)^3} \frac{k^2}{2m} \left(1 - \frac{\epsilon_k}{E_k}\right),$$

$$v_r(\alpha, \mu_{\text{eff}}, \Delta) = \int \frac{d^3\vec{k}}{(2\pi)^3} \frac{\Delta}{2E_k}.$$

The notation $\int \frac{d^3\vec{k}}{(2\pi)^3}$ represents either a discrete summation over box momenta $k_i = 2\pi m_i/L_i$ or the continuous integral $\int d^3\vec{k}/(2\pi)^3$ in the thermodynamic limit. The regulated quantities τ_r and v_r follow from these by subtracting the power-law divergences (this is equivalent to using dimensional regularization [43]):

$$\frac{\tau_r}{2m} = \int \frac{d^3\vec{k}}{(2\pi)^3} \frac{k^2}{2m} \left(1 - \frac{\epsilon_k}{E_k}\right) - \int \frac{d^3\vec{k}}{(2\pi)^3} \frac{m\Delta^2}{\alpha^2 k^2},$$

$$v_r = \int \frac{d^3\vec{k}}{(2\pi)^3} \frac{\Delta}{2E_k} - \int \frac{d^3\vec{k}}{(2\pi)^3} \frac{m\Delta}{\alpha k^2}.$$

Note that the subtraction integrals are continuous. In order to implement this regularization scheme in the periodic box, one must use a simultaneous spherical

cutoff on both the discrete and continuous momenta. The partial sums as a function of cutoff will fluctuate as various lattice points enter the sphere, but the magnitude of the fluctuations will reduce and the resulting limit converges. Numerically, it is favorable to sum over cubic shells so that the sequence of partial sums behaves smoothly, allowing one to accelerate the convergence. However, the location of the cutoff between shells must be fine tuned to reproduce the correct result because – unlike the spherical case – the fluctuations never die away with a cubic cutoff.

From the integrals one can see that the effective mass can be scaled out to define the following finite functions:

$$n_+ \left(\frac{\Delta}{\alpha}, \frac{\mu_{\text{eff}}}{\alpha} \right) = n_+(\alpha, \mu_{\text{eff}}, \Delta),$$

$$\tilde{C} \left(\frac{\Delta}{\alpha}, \frac{\mu_{\text{eff}}}{\alpha} \right) = -\frac{\alpha}{\Delta} v_r(\alpha, \mu_{\text{eff}}, \Delta),$$

$$\tilde{D} \left(\frac{\Delta}{\alpha}, \frac{\mu_{\text{eff}}}{\alpha} \right) = \frac{\alpha^2}{\Delta^2} \tau_r(\alpha, \mu_{\text{eff}}, \Delta).$$

One can thus deduce that, if the volume $V = L_x L_y L_z$ and shape of the box \vec{L} are held fixed, then the TF equations exhibit an additional invariance under scaling α , μ_{eff} , and Δ by the same factor

$$\frac{d\alpha}{\alpha} = \frac{d\mu_{\text{eff}}}{\mu_{\text{eff}}} = \frac{d\Delta}{\Delta}.$$

Note that this does not follow from dimensional analysis (α is already dimensionless) and expresses a non-trivial property of the TF equations. These scaling relationships allow us to express everything in terms of two dimensionless parameters – $\varkappa = \eta/\alpha$, and the total (dimensionless) particle number $N_+ = V n_+$ – through the dimensionless functions $c(\varkappa, N_+)$ and $d(\varkappa, N_+)$:

$$\varkappa \equiv \frac{\eta}{\alpha}, \quad N_+ \equiv n_+ V,$$

$$c(\varkappa, N_+) = \tilde{C} \frac{E_F^2}{\varepsilon_{FG}}, \quad d(\varkappa, N_+) = \tilde{D} \frac{E_F^2}{\varepsilon_{FG}},$$

$$v_r = -\frac{3\varkappa}{5} c(\varkappa, N_+) n_+, \quad \tau_r = \varkappa^2 d(\varkappa, N_+) \varepsilon_{FG}.$$

In the $T = 0$ thermodynamic limit $L \rightarrow \infty$ ($N_+ \rightarrow \infty$), the integrals can be performed analytically (see [43]). We start by defining:

$$k_0 = \sqrt{\frac{2m|\mu_{\text{eff}}|}{\alpha \hbar^2}}, \quad y_0 = \frac{\mu_{\text{eff}}}{\sqrt{\Delta^2 + \mu_{\text{eff}}^2}}.$$

We may then express our previous results as

$$n_+ = \frac{k_0^3}{3\pi^2} h_n, \quad \tilde{C} = \frac{mk_0}{4\pi\hbar^2} h_c, \quad \tilde{D} = \frac{-\alpha^2 \hbar^2 k_0^5}{8m\pi^2 \Delta^2} h_d,$$

where the functions h_n , h_c , and h_d depend only on y_0 ,

$$h_n(y_0) = \frac{3}{4} \frac{y_0 f_{1/2}(y_0) - f_{3/2}(y_0)}{|y_0|^{3/2}}, \quad h_c(y_0) = \frac{f_{1/2}(y_0)}{\pi |y_0|^{1/2}},$$

$$h_d(y_0) = \frac{f_{5/2}(y_0) - y_0 f_{3/2}(y_0)}{|y_0|^{5/2}}, \quad f_\alpha(y_0) = \frac{-\pi P_\alpha(-y_0)}{\sin(\pi\alpha)},$$

through the Legendre function $P_\alpha(x)$ which satisfies

$$0 = (1-x^2)P_\alpha'' - 2xP_\alpha' + \alpha(\alpha+1)P_\alpha,$$

$$P_\alpha(x) = \frac{1}{2\pi i} \oint \omega^{-\alpha-1} \sqrt{1-2x\omega+\omega^2} d\omega.$$

Noting that $n_+ = k_F^3/3\pi^2$ we can identify $k_F^3 = k_0^3 h_n$ and $E_F = \hbar^2 k_F^2/2m = h_n^{2/3} k_0^2/2m = h_n^{2/3} |\mu_{\text{eff}}|/\alpha$. We can then relate \aleph directly to y_0 through the monotonic function:

$$\aleph(y_0) = \frac{\Delta}{\alpha E_F} = \frac{\Delta}{|\mu_{\text{eff}}| h_n^{2/3}(y_0)} = \frac{\sqrt{y_0^{-2} - 1}}{h_n^{2/3}(y_0)}.$$

This function has the limiting behavior:

$$\aleph = \begin{cases} \left(\frac{4}{1+y_0} \right)^{1/6} & \text{where } y_0 \approx -1, \\ \sqrt{2(1-y_0)} & \text{where } y_0 \approx 1, \end{cases}$$

and an application of five steps of Newton's method using this as a guess (splitting the input at the point $\aleph \approx 1.211292490$ where these asymptotic forms meet) solves the inverse problem $y_0(\aleph)$ to machine precision. With this conversion we can directly express

$$c(\aleph) = c_{N_+=\infty}(\aleph) = \frac{5\pi}{8} \frac{h_c(y_0)}{h_n^{1/3}(y_0)},$$

$$d(\aleph) = d_{N_+=\infty}(\aleph) = \frac{-5}{4\aleph^2} \frac{h_d(y_0)}{h_n^{5/3}(y_0)},$$

allowing the parameters α , β , and γ to be computed from the thermodynamic values of α , ξ , and η :

$$\gamma = \frac{5\alpha(3\pi^2)^{2/3}}{6c(\eta/\alpha)}, \quad (\text{A4a})$$

$$\beta = \xi - \frac{d(\eta/\alpha)\eta^2}{\alpha} - \frac{6\eta^2\gamma}{5(3\pi^2)^{2/3}}. \quad (\text{A4b})$$

We use these equations to express all of our results in terms of the thermodynamic values of α , ξ , and η , even though the functional is expressed in terms of fixed parameters α , β , and γ .

Appendix B: Particles in a Box

Here we present some details about computing the energies E of $N_+ = N_a + N_b$ particles in a cubic box of size L^3 . There are two conventions for expressing the

energy of a box. We use $\xi_{N_+} = \mathcal{E}(N_+)/\mathcal{E}_{FG}$ where $\mathcal{E}(N_+) = E(N_+)/L^3$. All values of ξ reported in this paper have been converted to this normalization. The other convention $\xi^{\text{box}} = E(N_+)/E_{FG}(N_+)$ normalizes the energy with respect to the energy of N_+ non-interacting fermions in the same box (see [3] for conversion factors).

To further constrain our fits, we include the results for $N_+ = 2$. By solving the Schrödinger equation for two particles in a periodic box of size L^3 with the short-range boundary condition

$$\lim_{r \rightarrow 0} \Psi(\vec{x}, \vec{x} + \vec{r}) \propto \frac{1}{r} + k \cot \delta_k + \mathcal{O}(r),$$

one obtains

$$k \cot \delta_k = \frac{1}{\pi L} S \left(\left(\frac{Lk}{2\pi} \right)^2 \right),$$

$$S(\eta) = \lim_{\Lambda \rightarrow \infty} \sum_{\vec{n}}^{\Lambda} \frac{1}{\|\vec{n}\|^2 - \eta} - 4\pi\Lambda.$$

where $E = k^2/2m_r$ is the energy in the center-of-mass-frame and $m_r = m/2$ is the reduced mass of the system (see for example [44] and references therein). Note that for non-interacting particles, $E_{FG}(N_+) = 0$, thus for all attractive interactions, $E \propto k^2 < 0$. This poses no problems since only k^2 enters the formulation: for example, $k \cot \delta_k$ is a series in k^2 (1).

As before, the summation may be performed with partial sums over cubic shells: these behave smoothly and are amenable to series acceleration techniques (see [45] for example) such as the Levin transformation.

The energies $\xi_2(k_F r)$ are shown in figure 5 for the potentials (4). Over the ranges considered, the results are virtually identical. Finally, we note that the $N_+ = 2$ solution to the SLDA has only the normal solution $\Delta = 0$. Both particles enter the $k = 0$ ground state which has zero energy, hence we can identify $\beta(k_F r) = \xi_2(k_F r)$.

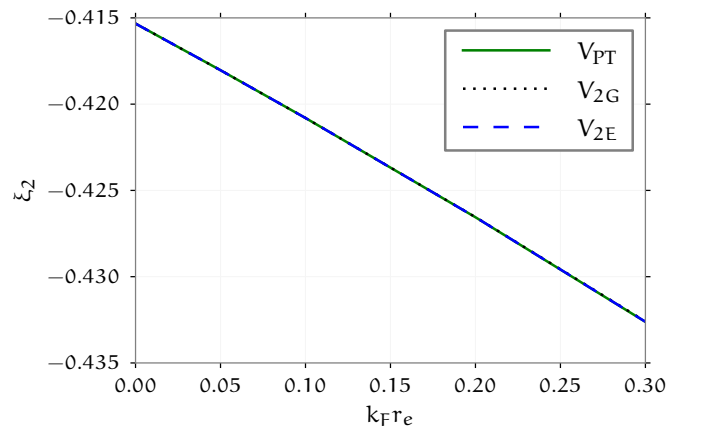


Figure 5. (color online) Exact ground-state energy $\xi_2(k_F r_e)$ for the $N_+ = 2$ system in a box for each of the potentials (4).

- [1] M. Inguscio, W. Ketterle, and C. Salomon, eds., *Ultra-cold Fermi Gases*, International School of Physics “Enrico Fermi”, Vol. 164 (IOS Press, Amsterdam, 2007); S. Giorgini, L. P. Pitaevskii, and S. Stringari, *Rev. Mod. Phys.* **80**, 1215 (2008), arXiv:0706.3360; W. Zwerger, ed., *The BCS–BEC Crossover and the Unitary Fermi Gas*, Lecture Notes in Physics, Vol. 836 (Springer-Verlag, Berlin Heidelberg, 2012).
- [2] A. J. Morris, P. López Ríos, and R. J. Needs, *Phys. Rev. A* **81**, 033619 (2010), arXiv:0910.0720.
- [3] M. M. Forbes, S. Gandolfi, and A. Gezerlis, *Phys. Rev. Lett.* **106**, 235303 (2011), arXiv:1011.2197.
- [4] X. Li, J. Kolorenč, and L. Mitás, *Phys. Rev. A* **84**, 023615 (2011), arXiv:1105.1748.
- [5] J. Braun, S. Diehl, and M. M. Scherer, *Phys. Rev. A* **84**, 063616 (2011), arXiv:1109.1946.
- [6] A. Gezerlis and J. Carlson, *Phys. Rev. C* **77**, 032801 (2008), arXiv:0711.3006.
- [7] H. A. Bethe, *Phys. Rev.* **76**, 38 (1949).
- [8] “The Many-Body Challenge Problem (MBX) formulated by G. F. Bertsch in 1999,”; G. A. Baker, Jr., *Phys. Rev. C* **60**, 054311 (1999); *Recent Progress in Many-Body Theories*, Int. J. Mod. Phys. B Series on Advances in Quantum Many-Body Theory, **15**, 1314 (2001).
- [9] M. J. H. Ku, A. T. Sommer, L. W. Cheuk, and M. W. Zwierlein, *Science* **335**, 563 (2012), arXiv:1110.3309.
- [10] M. Bartenstein, A. Altmeyer, S. Riedl, R. Geursen, S. Jochim, C. Chin, J. H. Denschlag, R. Grimm, A. Simoni, E. Tiesinga, C. J. Williams, and P. S. Julienne, *Phys. Rev. Lett.* **94**, 103201 (2005), arXiv:cond-mat/0408673.
- [11] D. E. Gonzalez Trotter, F. S. Meneses, W. Tornow, C. R. Howell, Q. Chen, A. S. Crowell, C. D. Roper, R. L. Walter, D. Schmidt, H. Witała, W. Glöckle, H. Tang, Z. Zhou, and I. Šlaus, *Phys. Rev. C* **73**, 034001 (2006); Q. Chen, C. R. Howell, T. S. Carman, W. R. Gibbs, B. F. Gibson, A. Hussein, M. R. Kiser, G. Mertens, C. F. Moore, C. Morris, A. Obst, E. Pasyuk, C. D. Roper, F. Salinas, H. R. Setze, I. Slaus, S. Sterbenz, W. Tornow, R. L. Walter, C. R. Whiteley, and M. Whitton, *Phys. Rev. C* **77**, 054002 (2008).
- [12] G. A. Miller, B. M. K. Nefkens, and I. Ålaus, *Phys. Rep.* **194**, 1 (1990).
- [13] S. Tan, (2005), arXiv:cond-mat/0505615; *Ann. Phys. (NY)* **323**, 2952 (2008), arXiv:cond-mat/0505200; *Ann. Phys. (NY)* **323**, 2971 (2008), arXiv:cond-mat/0508320.
- [14] A. Schwenk and C. J. Pethick, *Phys. Rev. Lett.* **95**, 160401 (2005), arXiv:nucl-th/0506042.
- [15] S. Simonucci, G. Garberoglio, and S. Taioli, *Phys. Rev. A* **84**, 043639 (2011), arXiv:1110.1441.
- [16] S. F. Caballero-Benitez, R. Paredes, and V. Romero-Rochin, “The Contact in the BCS-BEC crossover for finite range interatomic potentials,” (2012), arXiv:1202.2939.
- [17] J. Carlson, S.-Y. Chang, V. R. Pandharipande, and K. E. Schmidt, *Phys. Rev. Lett.* **91**, 050401 (2003), arXiv:physics/0303094.
- [18] S. Gandolfi, K. E. Schmidt, and J. Carlson, *Phys. Rev. A* **83**, 041601 (2011), arXiv:1012.4417.
- [19] S. Sorella, *Phys. Rev. B* **64**, 024512 (2001), arXiv:cond-mat/0009149.
- [20] J. Carlson, S. Gandolfi, K. E. Schmidt, and S. Zhang, *Phys. Rev. A* **84**, 061602 (2011), arXiv:1107.5848.
- [21] T. Papenbrock, *Phys. Rev. A* **72**, 041603 (2005), arXiv:cond-mat/0507183.
- [22] G. Rupak and T. Schaefer, *Nucl. Phys.* **A816**, 52 (2009), arXiv:0804.2678.
- [23] L. Salasnich and F. Toigo, *Phys. Rev. A* **78**, 053626 (2008), arXiv:0809.1820.
- [24] A. Bulgac, *Phys. Rev. A* **76**, 040502 (2007), arXiv:cond-mat/0703526.
- [25] A. Bulgac, M. M. Forbes, and P. Magierski, “The Unitary Fermi Gas: From Monte Carlo to Density Functionals,” Chap. 9, pp. 305 – 373, vol. 836 of [1] (2012), arXiv:1008.3933.
- [26] M. M. Forbes, “The unitary fermi gas in a harmonic trap and its static response,” (in prep.) (2012).
- [27] S. Tan, Private communication.
- [28] J. Bergstra, O. Breuleux, F. Bastien, P. Lamblin, R. Pascanu, G. Desjardins, J. Turian, D. Warde-Farley, and Y. Bengio, in *Proceedings of the Python for Scientific Computing Conference (SciPy)* (2010) oral Presentation.
- [29] J. Carlson and S. Reddy, *Phys. Rev. Lett.* **95**, 060401 (2005), arXiv:cond-mat/0503256.
- [30] A. Bulgac and M. M. Forbes, *Phys. Rev. Lett.* **101**, 215301 (2008), arXiv:0804.3364 [cond-mat].
- [31] J. Carlson and S. Reddy, *Phys. Rev. Lett.* **100**, 150403 (2008), arXiv:0711.0414 [cond-mat].
- [32] A. Schirotzek, Y. Shin, C. H. Schunck, and W. Ketterle, *Phys. Rev. Lett.* **101**, 140403 (2008), arXiv:0808.0026v2.
- [33] F. Werner and Y. Castin, *Phys. Rev. A* **86**, 013626 (2012), arXiv:1204.3204; Y. Castin and F. Werner, “The Unitary Gas and its Symmetry Properties,” Chap. 5, vol. 836 of [1] (2011), arXiv:1103.2851; F. Werner and Y. Castin, “Exact relations for quantum-mechanical few-body and many-body problems with short-range interactions in two and three dimensions,” (2010), arXiv:1001.0774.
- [34] A. Bhattacharyya and T. Papenbrock, *Phys. Rev. A* **74**, 041602 (2006), arXiv:nucl-th/0602050.
- [35] S. Bour, X. Li, D. Lee, U.-G. Meißner, and L. Mitás, *Phys. Rev. A* **83**, 063619 (2011), arXiv:1104.2102.
- [36] A. Gezerlis, (2008), unpublished.
- [37] S. Gandolfi, J. Carlson, and S. C. Pieper, *Phys. Rev. Lett.* **106**, 012501 (2011), arXiv:1010.4583.
- [38] D. T. Son and M. B. Wingate, *Ann. Phys. (NY)* **321**, 197 (2006), arXiv:cond-mat/0509786.
- [39] D. Blume and K. M. Daily, *C. R. Phys.* **12**, 86 (2011), arXiv:1008.3191.
- [40] D. Blume, J. von Stecher, and C. H. Greene, *Phys. Rev. Lett.* **99**, 233201 (2007), arXiv:0708.2734 [cond-mat].
- [41] S. Gandolfi, J. Carlson, and K. E. Schmidt, unpublished (2010).
- [42] S.-Y. Chang and G. F. Bertsch, *Phys. Rev. A* **76**, 021603 (2007), arXiv:physics/0703190.
- [43] T. Papenbrock and G. F. Bertsch, *Phys. Rev. C* **59**, 2052 (1999), nucl-th/9811077.
- [44] S. R. Beane, P. F. Bedaque, A. Parreño, and M. J. Savage, *Phys. Lett. B* **585**, 106 (2004), arXiv:hep-lat/0312004.
- [45] F. Bornemann, D. Laurie, S. Wagon, and J. Waldvogel, *The SIAM 100-Digit Challenge* (SIAM, Philadelphia, 2004).